



HAL
open science

Experimental investigation of the effect of the Reynolds number on the performance of a micro-scale and low tip-speed ratio wind turbine

Martin Bourhis, Michaël Pereira, Florent Ravelet

► **To cite this version:**

Martin Bourhis, Michaël Pereira, Florent Ravelet. Experimental investigation of the effect of the Reynolds number on the performance of a micro-scale and low tip-speed ratio wind turbine. 16th International Conference on Heat Transfer, Fluid Mechanics and Thermodynamics (HEFAT2022), Aug 2022, Amsterdam, Netherlands. pp.438-443. hal-03763339v2

HAL Id: hal-03763339

<https://hal.science/hal-03763339v2>

Submitted on 30 Aug 2022

HAL is a multi-disciplinary open access archive for the deposit and dissemination of scientific research documents, whether they are published or not. The documents may come from teaching and research institutions in France or abroad, or from public or private research centers.

L'archive ouverte pluridisciplinaire **HAL**, est destinée au dépôt et à la diffusion de documents scientifiques de niveau recherche, publiés ou non, émanant des établissements d'enseignement et de recherche français ou étrangers, des laboratoires publics ou privés.

EXPERIMENTAL INVESTIGATION OF THE EFFECT OF THE REYNOLDS NUMBER ON THE PERFORMANCE OF A MICRO-SCALE AND LOW TIP-SPEED RATIO WIND TURBINE

Bourhis M.* and Pereira M. and Ravelet F.

*Author for correspondence

Laboratory of Fluid Engineering and Energy Systems,
Arts et Metiers Institute of Technology, CNAM, LIFSE, HESAM University,
Paris, 75013,
France,
E-mail: martin.bourhis@ensam.eu

ABSTRACT

Micro-scale wind turbines are of great interest to supply rechargeable batteries of autonomous sensors in the field of the Internet Of Things (IOT). However, they face the issue of lower dimensionless performance than large-scale wind turbines. Due to their small size and low operating wind speed, these runners operate mainly in low Reynolds number flow conditions at which the aerodynamic properties of the blades are not well-known. Even though promising results are reported on the Reynolds number effects on isolated and non rotating blades, their applicability to design efficient small rotating energy harvesters is questionable. This paper reports on the influence of the Reynolds number on the performance of high-solidity and low tip-speed ratio micro-scale wind turbines. Wind turbine's power and torque coefficient vs. tip-speed ratio curves are measured in wind tunnel for a wide range of Reynolds number by changing either the turbine's diameter or the freestream wind velocity. This quantitative analysis will contribute to design more efficient wind energy harvesters.

INTRODUCTION

The current fast development of Internet of Things (IOT) devices raises the question of their supply in power. IOT appliances such as wireless monitoring sensors, are supposed to be deployed everywhere and to be accessible any time from anywhere, hence it implies high requirements for energy storage and power management [1]. Currently, batteries are widely used to power autonomous sensors but their use presents major drawbacks. The finite amount of energy available, the high cost of replacement or the possible difficulties to have access to it in hazardous locations for maintenance limit the spread of these devices. The use of ambient sources such as solar energy, thermal energy or mechanical energy could be considered as a solution to reduce or eliminate batteries in IOT endpoints. Wind energy is one of the available renewable resource of energy. Even though wind power is highly intermittent, a recent study carried out by Wen et al. emphasises that the average wind speed in major Chinese

NOMENCLATURE

C_p	[-]	Power coefficient
$C_{p,max}$	[-]	Maximum power coefficient
P	[W]	Mechanical power
P_a	[W]	Available power
τ	[N.m]	Torque
ω	[rad.s ⁻¹]	Angular velocity
ρ	[kg.m ⁻³]	Air density
R_T	[m]	Tip radius
V_∞	[m.s ⁻¹]	Freestream wind velocity
Re	[-]	Reynolds number
c	[m]	Blade chord length
W	[m.s ⁻¹]	Relative velocity
η	[Pa.s]	Dynamic viscosity of air
C_τ	[-]	Torque coefficient
λ	[-]	Tip-speed ratio
λ_{opt}	[-]	Optimum tip-speed ratio
C_l	[-]	Lift coefficient
C_d	[-]	Drag coefficient
N	[-]	Number of blades
R_H	[m]	Hub radius
H	[-]	Hub ratio
a	[-]	Axial induction factor
C	[m.s ⁻¹]	Absolute velocity
C_θ	[m.s ⁻¹]	Tangential velocity
C_z	[m.s ⁻¹]	Axial velocity
σ	[-]	Blade solidity
ϕ	[deg]	Blade pitch angle
β	[deg]	Relative angle
α	[deg]	Angle of attack
l	[m]	Blade spacing

cities is essentially within the range of 1 m.s⁻¹ to 7 m.s⁻¹ [2]. Consequently, miniature wind energy harvesters, such as micro-scale wind turbines, could collect the energy of low speed airflow in urban area to power a rechargeable battery or a capacitor [3].

Micro-scale runners, with a rotor diameter under 0.20 m, are not currently widely used because they achieve low efficiency *i.e.* low maximum power coefficient $C_{p,max}$, especially in comparison with full-scale wind turbines. The power coefficient C_p is defined as the ratio of the mechanical power P to the available power P_a :

$$C_p = \frac{P}{P_a} = \frac{\tau\omega}{0.5\rho\pi R_T^2 V_\infty^3} \quad (1)$$

where τ is the torque, ω is the angular velocity, R_T is the tip radius of the rotor, ρ is the air density and V_∞ is the freestream wind velocity. It can be observed from the literature that the maximum power coefficient $C_{p,max}$ drops as the rotor diameter decreases. Most small wind turbines exhibit maximum power coefficient $C_{p,max} \leq 0.3$ while large scale rotors achieve $C_{p,max}$ close to 0.5.

As the rotor diameter is small and the operating freestream is low, micro-scale runners operate mainly in low Reynolds number flow conditions ($Re \leq 10^5$). In this study, the Reynolds number Re is based on the chord length c and on the relative velocity W and reads :

$$Re = \frac{\rho W c}{\eta} \quad (2)$$

where η is dynamic viscosity of air.

The effects of the Reynolds number on the power coefficient C_p and torque coefficient C_τ is barely addressed in the literature. However, it is of particular interest to deeply understand flow behaviour around a rotor in order to design more efficient runners. The torque coefficient C_τ is a dimensionless measure of the torque generated by a rotor and reads :

$$C_\tau = \frac{\tau}{0.5\rho\pi R_T^3 V_\infty^2} \quad (3)$$

Some experimental studies have found that runner's performance and wake were affected by the Reynolds number, especially at low Reynolds number. McTavish et al. have shown that the thrust coefficient and the wake expansion downstream a 25 cm wind turbine increase with increasing Reynolds number [4]. Cunningham et al. performed on field test with a low-solidity 3.74 m diameter horizontal axis wind turbine [5]. Their results show a significant drop in the wind turbine's power coefficient and an increase in the optimum tip-speed ratio λ_{opt} as Reynolds number decreased. The authors reported that the dependency of the C_p vs. λ curves on Reynold's number was induced by the variations of the rotor's aerodynamic lift and drag coefficients with the Reynolds number. Another experimental study carried out by Kadrowski et al. reveals also that higher Reynolds numbers allows the turbine to reach higher maximum power coefficient $C_{p,max}$ but at lower optimum tip-speed ratio λ_{opt} [6]. Wiesner [7] and Capata & Sciubba [8] performed analytical and numerical investigation of the Reynolds numbers effects on centrifugal compressor and turbocompressor performance and derived efficiency/ Re correlation formula. However, to date there are no such correlations for wind turbines and there is no consensual agreement on the effects of low Reynolds number on micro-scale wind turbine's performance.

Wind turbine's blades ensure the conversion of the kinetic power of the wind into mechanical power, hence their geometry is closely linked to the flow patterns and to the rotor's performance. The classical method to design wind turbine's blades is

called the Blade Element Momentum Theory. Firstly, once determined a design tip-speed ratio, optimum flow conditions are computed from the general momentum theory [9]. In the general momentum theory, the rotor is modelled as an actuator disc *i.e.* a rotor with an infinite number of blades, inducing a sudden pressure jump. As the thrust force acting over the rotor is function of the pressure drop, so does the power coefficient. One limitation of the actuator disc theory is that the physical behaviour of the blades is not modelled. Consequently, the optimum flow conditions and the maximum power coefficient of a wind turbine are theoretically not sensitive to a change in the Reynolds number.

Secondly, the chord length and pitch angle distributions are computed in order to achieve the thrust force derived from the general momentum theory. The classical method is based on 2D lift and drag coefficients obtained from wind tunnel experiments performed in high Reynolds number flow conditions with isolated and non-rotating airfoils. Existing research recognises the critical role played by the Reynolds number on the flow pattern around an isolated airfoil and its aerodynamic properties. It is well acknowledged that an increase in Re leads to an increase in the lift coefficient C_l and stall angle and a decrease in the drag coefficient C_d [10]. However, the variation of the optimum angle of attack *i.e.* the angle of attack which produces the higher C_l/C_d ratio is highly dependent on the airfoil geometry.

Even though the findings on isolated airfoils are useful to understand Reynolds number effects on large-scale rotor aerodynamics, some limitations occur when the rotor diameter or the operating wind speed decrease. Indeed, the blades of micro-scale wind turbines are affected by additional parameters such as low Reynolds numbers effects and rotating effects [11]. Moreover, micro-scale turbines require high-blade solidity in order to increase the torque at low freestream wind velocity and to start rotating. The mutual blade interaction induces by the increase in blade solidity may affect the formation of laminar separation bubbles in the closely spaced blades [12]. Consequently, the effects of the Reynolds number on the performance of high-solidity blade cascade in rotation may differ from those observed with isolated airfoils [13].

Therefore, the purpose of the current study is to evaluate the effect of the Reynolds number on the power coefficient C_p and torque coefficient C_τ with high-solidity and low tip-speed ratio wind turbines. In order to cover a wide range of Reynolds numbers, three geometrically scaled turbines were designed and tested in wind tunnel under various upcoming wind velocities.

DESIGN OF THE TURBINES

Three high-solidity and low tip-speed ratio runners with diameters equal to 300 mm, 200 mm and 100 mm and identical relative geometries were designed. All turbines' dimensionless parameters are equal in order to get a pure geometrical scaling. The design procedure of the 300 mm runner has been the subject of a preliminary study [14], hence only some relevant design steps are documented in this paper. As reported in Ref.[14], this runner achieves a high maximum power coefficient at its design tip-speed ratio $C_{p,max}(\lambda = 1) = 0.31$ for a freestream wind

velocity $V_\infty = 10 \text{ m.s}^{-1}$. Moreover, its torque coefficient C_τ decreases linearly with the tip-speed ratio and it has a very low cut-in wind speed. These specificities make this turbine a good energy harvester. Consequently, the geometries of the 200 mm and 100 mm runners are obtained by scaling this 300 mm rotor.

The runners have $N = 8$ blades, a hub ratio $H = R_H/R_T$ equal to $H = 0.3$ and a design tip-speed ratio $\lambda = 1$. The blade was discretized into 11 elements from the root (R_H) to the tip (R_T) of the blades. For each radius, a circular camber-mean line which is tangent to the relative velocity at the leading edge \vec{W}_1 and at the trailing edge \vec{W}_2 was drawn and thickened with NACA0010 profiles (see Fig.1). The relative velocities at the design tip-speed ratio were predicted by applying the Euler's turbomachinery theorem and the axial momentum theory to a disc of streamtube with the hypothesis of a uniform and purely axial discharging flow $C_1 = V_\infty(1 - a)$ with $a = 1/3$ and a constant vortex law C_{02} . The full calculation procedure for the relative velocities can be found in Ref.[14].

At $\lambda = 1$, the inlet and outlet relative angle decreases from $\beta_1 = 66^\circ$ and $\beta_2 = 35^\circ$ at the hub to $\beta_1 = 34^\circ$ and $\beta_2 = 26^\circ$ at the tip. The blade pitch angle ϕ , defined as the angle between the chord line and the rotor's plane, varies from $\phi = 55^\circ$ at the hub to $\phi = 30^\circ$ at the tip. Hub and tip chord lengths were calculated according to $c = 2\pi r\sigma/N$ with a blade solidity at the hub $\sigma(R_H) = 1.65$ and $\sigma(R_T) = 0.7$ at the tip. The chord length for each radii was then determined by assuming a linear variation from hub to tip. Finally, the rotors were manufactured by fused material deposition with polyactic acid filament. The printed rotors are shown in Fig.2.

DESCRIPTION OF THE EXPERIMENTAL SETUP

The aim of the experimental investigation is to determine the power coefficient C_p and torque coefficient C_τ , vs. tip-speed ratio λ characteristics for various Reynolds number by changing either the runner or the freestream wind velocity V_∞ between acquisitions.

The experiments were carried out in the wind tunnel of the LIFSE facilities. This closed-loop wind tunnel has a 1.8 m

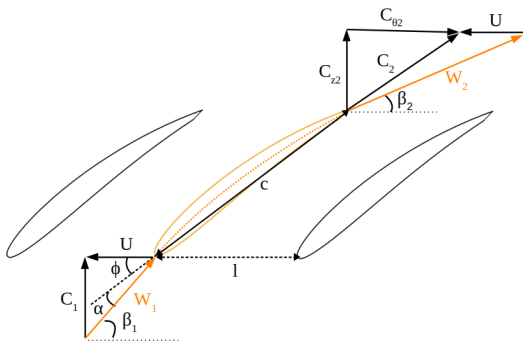


Figure 1: From Bourhis et al. [14]. Velocity triangles at the inlet (index 1) and outlet (index 2) of the turbine cascade. The blade solidity σ is defined as the ratio of the blade chord length c with spacing l i.e. $\sigma = c/l$



Figure 2: Printed wind turbines used in scaling tests with a 50 euro cent coin

long semi-open test section with a $1.35 \text{ m} \times 1.65 \text{ m}$ cross-section. Prior to data acquisition, the atmospheric pressure and the temperature were systematically measured to compute the daily air density. The freestream wind speed V_∞ was computed through the measurements of the dynamic pressure in the test section by a pitot transducer Furness Control FC20. The torque τ and the angular velocity ω were acquired using a torque transducer located between the turbine and a DC generator. These measuring devices were housed in a nacelle placed in the middle of the test section. A detailed schematic of the experimental setup with the 300 mm runner mounted on its nacelle is displayed in Fig.3.

An increase in the rotor diameter or in the upcoming wind speed induces an increase in the aerodynamic torque. Therefore, in order to extend the range of measurable torque, two nacelles including torque meters with different measuring ranges were built. On one hand, the torque generated by the 300 mm runner and 200 mm runner were measured by a rotating torque meter HBM-T20WN. It has a measuring range of 0 N.m to 2 N.m and an accuracy of 0.2% of full scale. On the other hand, a second nacelle containing a rotating torque meter DRVL with a smaller measuring range was used to acquire the torque and the angular velocity of the 100 mm rotor. The latter has a measuring range of 0 N.m to 0.05 N.m and a maximum measurement error

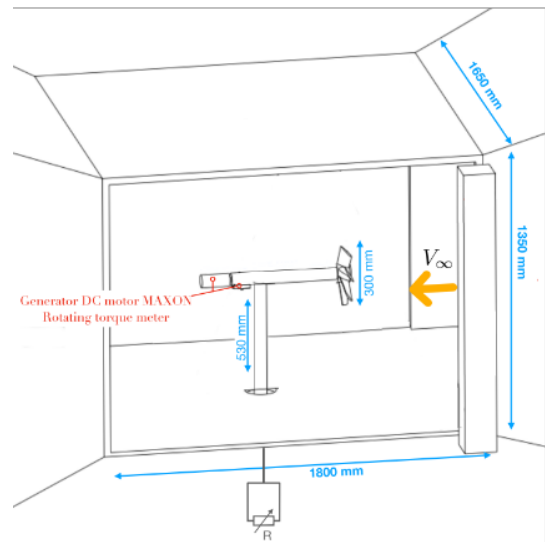


Figure 3: Detailed schematic of the experimental setup with the 300 mm wind turbine mounted on its nacelle

R_T	[mm]	50		100		150			
V_∞	[m.s ⁻¹]	10	15	10	15	10	15	20	25
$Re(R_H)$		9500	14200	18900	28400	28400	42600	56800	71100
$Re(R_T)$		22000	33000	44100	66100	66100	99100	132200	165200
Marker in plots		■	■	+	+	×	×	×	×

Table 1: Description of the experimental test conditions $\{R_T, V_\infty\}$. Reynolds numbers Re are computed at the hub ($Re(R_H)$) and at the tip of the blade ($Re(R_T)$) according to Eq.2. A specific marker, used to plot the experimental results, is assigned to each test condition

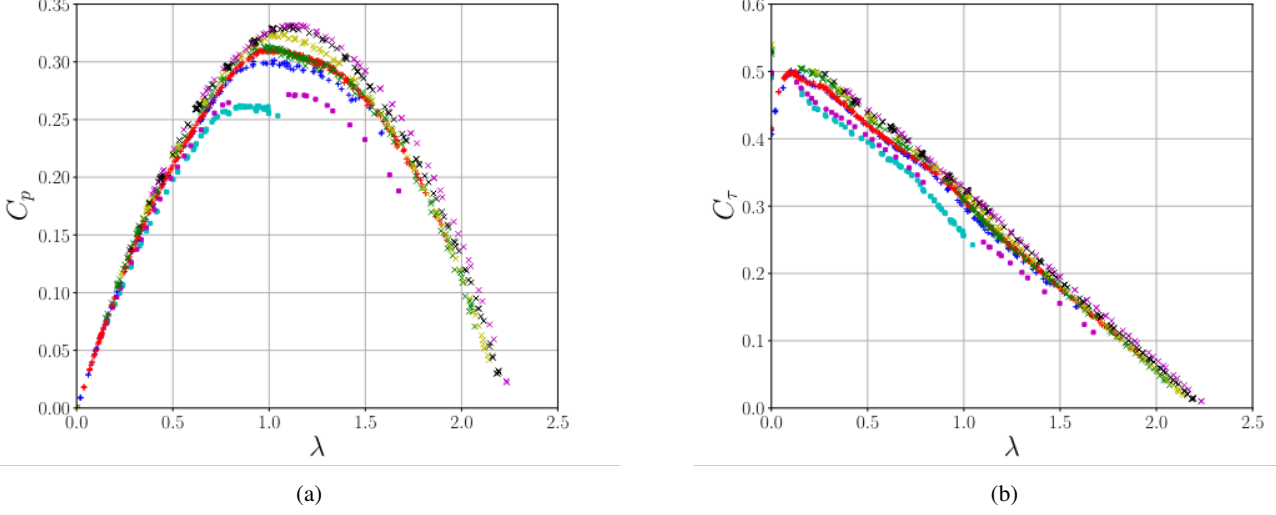


Figure 4: Power coefficient C_p (a) and torque coefficient C_τ (b) as a function of the tip-speed ratio λ for various Reynolds number (please see the Tab.1). The curves are obtained from the gathering of several experimental data sets for each $\{R_T, V_\infty\}$ configuration

of 0.15% of full scale. The different test conditions are shown in the first two rows of Tab.1. For each rotor, the range of upcoming wind velocity was limited by the measurement capabilities of the torque transducers.

During an acquisition, the upstream flow velocity V_∞ was kept constant while the rotational speed of the rotor ω *i.e.* the operating tip-speed ratio λ varied between each sample by changing the resistive load applied to the generator. For each sample, the arithmetic mean value of the torque τ , the angular velocity ω , the temperature and the dynamic pressure in the test section were collected from 50 s long acquisitions with a sampling frequency of 1000 Hz. Then, the torque coefficient and power coefficient were computed for each sample according to the Eqs.1&3. The experiments were repeated several times for the different set of conditions on separate days to ensure repeatability of the acquisition protocol. Finally, the data were gathered and displayed on a single graph showing the variations of C_p and C_τ with the tip-speed ratio for each test conditions.

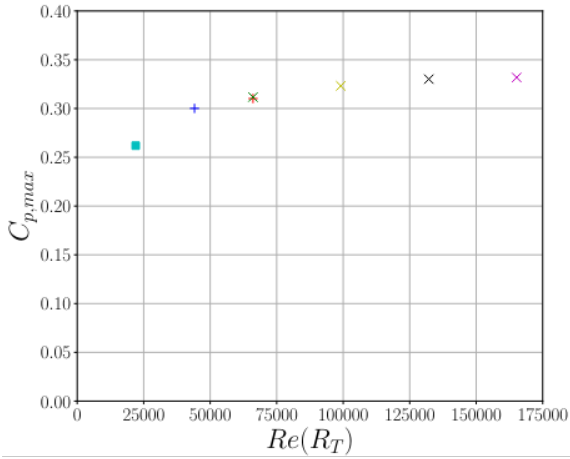
The Reynolds number, Re , for each experimental configurations $\{R_T, V_\infty\}$ was calculated for analysis and is displayed in Tab.1. The latter is computed at the hub ($r = R_H$) and at the tip ($r = R_T$) of the blades according to the Eq.2 where $W = \sqrt{(2/3V_\infty)^2 + (r\omega)^2}$, $\rho = 1.2 \text{ kg.m}^{-3}$, $\eta = 1.8.10^{-5} \text{ Pa.s}$ and $\lambda = 1$. The range of tip Reynolds numbers extend from $Re = 22000$ (■) for the configuration $\{50, 10\}$ to $Re = 165200$

(×) for the configuration $\{150, 25\}$. As shown in Tab.1, the 300 mm runner and 200 mm runner operate at the same Reynolds number when the upcoming wind velocity are respectively set at $V_\infty = 10 \text{ m.s}^{-1}$ (+) and $V_\infty = 15 \text{ m.s}^{-1}$ (×).

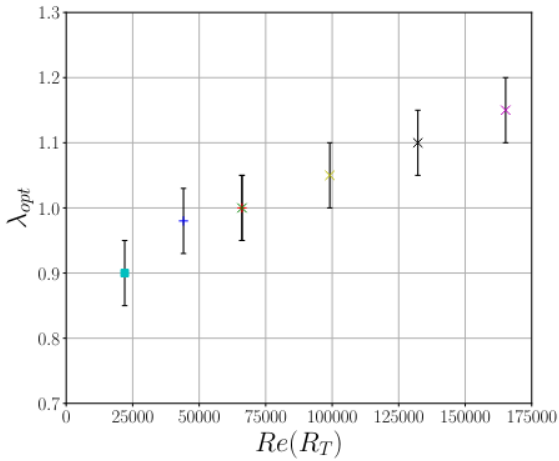
As the Reynolds number is computed with the relative velocity, a decrease in the tip-speed ratio leads to a decrease in Re . Therefore, in the following discussion, each $\{R_T, V_\infty\}$ configuration is identified by its tip Reynolds number computed at $\lambda = 1$ and by a specific marker in the experimental plots (see the last row of Tab.1).

RESULTS AND DISCUSSIONS

Fig.4 shows the variation of the power coefficient C_p and the variation of the torque coefficient C_τ as a function of the tip-speed ratio λ for the different test conditions. For all test conditions, the range of operating tip-speed ratio was limited either by the friction of the mechanical parts contain in the nacelle or by the capacity of the breaking system. No experimental power and torque coefficients were measured between $\lambda = 0.7$ and $\lambda = 1.1$ when the 100 mm rotor were operating at $V_\infty = 15 \text{ m.s}^{-1}$ (■) due to a strong resonance of the transmission shaft. Furthermore, when the 300 mm runner and 200 mm runner operate at the same Reynolds number (+ & ×) both C_p and C_τ vs. λ curves follow similar trends. In both test conditions, the same maximum power coefficient $C_{p,max} = 0.31$ for an equal optimum tip-speed ratio



(a)



(b)

Figure 5: Effect of the Reynolds number on the maximum power coefficient $C_{p,max}$ (a) and on the optimum tip-speed ratio λ_{opt} (b). The tip Reynolds number computed at $\lambda = 1$ is used as reference for the Re axis (see Tab.1)

$\lambda_{opt} = 1$. It emphasises that the dimension of the test section and the mechanical or electrical losses induce by the setup have no effect on the experimental measurements. The slight discrepancy in C_τ between these two test conditions at very low tip-speed ratio might be explained by rotational effects or by the difference of blade's relative rugosity.

The variation of the torque coefficient with the tip-speed ratio are consistent with preliminary results reported in Ref.[14]. For all tests performed with the 300 mm runner, the torque coefficient decreases linearly for the entire range of tip-speed ratio. Even though a similar trend is observed at high tip-speed ratio with the 200 mm and 100 mm turbines, a decrease in Re leads to a change in the C_τ vs. λ curves, especially at low tip-speed ratio.

Nonlinear variations and a little drop in C_τ are observed with the 200 mm and 100 mm turbines at tip-speed ratios close to $\lambda = 0$. A decrease in the tip-speed ratio leads to an increase in the angle of attack and a decrease in the Reynolds number. At high angles of attack, the lift curves can become highly nonlinear especially at low Reynolds number [15]. It can lead to nonlinear variations in C_τ at low tip-speed ratios.

Secondly, what stands out in the Fig.4b is the increase in C_τ with the Reynolds number for the entire range of tip-speed ratio. At fixed λ , all turbines operate with the same angle of attack α (see the velocity triangle in Fig.1), hence an increase in Re leads to an increase in the net aerodynamic forces acting on the wind turbine's blades. Even though, this finding is directly in line with the findings on isolated airfoils, a major difference is observed between the behaviour of an isolated airfoils and a blade cascade. For isolated airfoils, an increase in the angle of attack leads to an increase in the lift coefficient until the stall angle at which a sudden decrease in the lift generated by the aerofoil occurs. Interestingly, even at low Reynolds number, no significant drop in the torque coefficient is observed while decreasing the tip-speed ratio with high-solidity blade cascade. The stall effects may be counterbalanced by the mutual interaction between the blades.

As one can see in Fig.4a, the power coefficient C_p increases with increasing Reynolds number for the entire range of tip-speed ratio. However, higher Reynolds number leads to narrower C_p vs. λ curves. These results emphasize that the C_l/C_d vs. α curves of the rotating blade cascade change as the Re changes. An increase in Re induces a higher maximum C_l/C_d ratio and narrower C_l/C_d vs. α curves. It implies that the aerodynamic properties of the turbine's blades are more affected by a change in the angle of attack at high Reynolds number. Fig.5a highlights the gradual increase in the maximum power coefficient $C_{p,max}$ with the Reynolds number. For instance, the latter increases from $C_{p,max} = 0.26$ at $Re = 22000$ to $C_{p,max} = 0.33$ at $Re = 165200$. However, the difference in $C_{p,max}$ between each test conditions decreases with Re . The trend of the $C_{p,max}$ vs. λ curve suggests that the maximum power coefficient will probably level off or increases slowly. This finding is consistent with data reported on isolated airfoils [5; 16]. At high Reynolds number, the decrease in the lift coefficient and the increase in the drag coefficient of isolated airfoils are negligible. However, below a critical Reynolds number, C_l decreases fastly and C_d increases rapidly. $C_{p,max}$ vs. λ curve show a very similar pattern of results. It emphasises that the effect of the Reynolds number on the maximum power coefficient occurs mainly at $Re \leq 10^5$.

Fig.5b shows the variation of the optimal tip-speed ratio λ_{opt} with the Reynolds number. For all test conditions, the optimum tip-speed ratio is very close to the design tip-speed ratio $\lambda = 1$. As Figs.4a & 5b show, there is a clear trend of increasing optimum tip-speed ratio λ_{opt} with the Reynolds number. Even though the C_l/C_d remains quasi-constant for $Re \geq 10^5$, the optimum tip-speed ratio is continuously increasing.

The variations of the dimensionless parameters with the Reynolds number may be explained by the fact that in low

Reynolds number conditions $10^4 \leq Re \leq 10^6$, a too high adverse pressure gradient along the streamwise direction can lead to the separation of the boundary layer on the upper surface of the blades and the formation of laminar separation bubbles (LSB) inside which high recirculations of mixed laminar and turbulent flows occur [12]. For isolated airfoils, the size of the LSB, its position on the upper surface of the blade, its separation and reattachment coordinates and its effect on the lift and drag coefficients depend on the Reynolds number, the angle of attack, the turbulence intensity and the blade's roughness [17]. With micro-scale turbines, additional phenomena are involved in the formation of LSB such as rotational effects [11] and high blade solidity effects. Our results suggest that at fixed tip-speed ratio *i.e.* at fixed angle of attack, the overall length and thickness of laminar separation bubbles decreases as the Reynolds number increases. Moreover, the discrepancy in the C_τ vs. λ curves at low tip-speed ratios *i.e.* at very low Reynolds numbers and high angles of attack might be induced by changes in the flow regime. Further work should be undertaken to corroborates these findings. An investigation of the velocity fields in the near wake of a micro-scale turbine could provide a better understanding of the flow pattern around a rotating blade cascade operating at low Reynolds number and therefore could help to design more efficient wind energy harvesters.

CONCLUSION

The aim of the current study was to examine the effect of the Reynolds number on high-solidity micro-scale wind turbine's C_τ vs. λ curves and C_p vs. λ curves. The research has identified that an increase of the Reynolds number from $Re = 22000$ to $Re = 165200$ leads to an increase in the maximum power coefficient from $C_{p,max} = 0.26$ to $C_{p,max} = 0.33$. However, for $Re \geq 10^5$, $C_{p,max}$ remains quasi-constant. The second major finding was that higher Reynolds number flow conditions leads to higher torque coefficient C_τ and power coefficient C_p for the entire range of tip-speed ratio. Finally, these experiments have shown that the optimum tip-speed ratio *i.e.* the optimum angle of attack of the blade cascade increases as the Reynolds number increases. Even though, this study provide quantitative experimental data on the effect of the Reynolds number on the performance of micro-scale wind turbines, further experimental investigation are needed to fully understand its implications on the flow pattern around wind turbine's blades.

REFERENCES

- [1] Andrey Somov and Raffaele Giaffreda. Powering iot devices: Technologies and opportunities. *IEEE IoT Newsletter*, 2015.
- [2] Quan Wen, Xianming He, Zhuang Lu, Reinhard Streiter, and Thomas Otto. A comprehensive review of miniaturized wind energy harvesters. *Nano Materials Science*, 3(2):170–185, 2021. Nano Energy Materials and Devices for Miniaturized Electronics and Smart Systems.
- [3] Ali M. Eltamaly, Majed A. Alotaibi, Abdulrahman I. Alolah, and Mohamed A. Ahmed. Iot-based hybrid renewable energy system for smart campus. *Sustainability*, 13(15), 2021.
- [4] S. McTavish, Daniel Feszty, and F. Nitzsche. Evaluating reynolds number effects in small-scale wind turbine experiments. *Journal of Wind Engineering and Industrial Aerodynamics*, 120:81–90, 2013.
- [5] John Cunningham and Patrick Lemieux. *Study of Low Reynolds Number Effects on Small Wind Turbine Performance*.
- [6] Damian Kadrowski, Michal Kulak, Michal Lipian, Malgorzata Stepień, Piotr Baszczyński, Karol Zawadzki, and Maciej Karczewski. Challenging low reynolds - swt blade aerodynamics. *MATEC Web of Conferences*, 234:01004, 2018.
- [7] F. J. Wiesner. A New Appraisal of Reynolds Number Effects on Centrifugal Compressor Performance. *Journal of Engineering for Power*, 101(3):384–392, 1979.
- [8] Roberto Capata and Sciubba Enrico. Use of modified balje maps in the design of low reynolds number turbocompressors. volume 7, 2012.
- [9] JN. Sørensen. *General Momentum Theory for Horizontal Axis Wind Turbines*, volume 4 of *Research Topics in Wind Energy*. Springer International Publishing, Cham, 2016.
- [10] Justin Winslow, Hikaru Otsuka, Bharath Govindarajan, and Inderjit Chopra. Basic understanding of airfoil characteristics at low reynolds numbers (104–105). *Journal of Aircraft*, 55(3):1050–1061, 2018.
- [11] H. Himmelskamp, Aerodynamische Versuchsanstalt Göttingen, Great Britain. Ministry of Aircraft Production, and Luftfahrtforschungsanstalt Hermann Georing. *Profile Investigations on a Rotating Airscrew*. ARC-10856. Ministry of Aircraft Production, 1947.
- [12] P B S Lissaman. Low-Reynolds-Number Airfoils. *Annual Review of Fluid Mechanics*, 15(1):223–239, 1983.
- [13] D. J. Sharpe. A general momentum theory applied to an energy-extracting actuator disc. *Wind Energy*, 7(3):177–188, 2004.
- [14] M. Bourhis, M. Pereira, F. Ravelet, and I. Dobrev. Innovative design method and experimental investigation of a small-scale and very low tip-speed ratio wind turbine. *Experimental Thermal and Fluid Science*, 130:110504, 2022.
- [15] S Worasinchai, G Ingram, and R Dominy. A low-reynolds-number, high-angle-of-attack investigation of wind turbine aerofoils. *Proceedings of the Institution of Mechanical Engineers, Part A: Journal of Power and Energy*, 225(6):748–763, 2011.
- [16] Shubham Jain, Nekkanti Sitaram, and Sriram Krishnaswamy. Effect of reynolds number on aerodynamics of airfoil with gurney flap. *International Journal of Rotating Machinery*, 2015, 2015.
- [17] Tianyu Xia, Hao Dong, Liming Yang, Shicheng Liu, and Zhou Jin. Investigation on flow structure and aerodynamic characteristics over an airfoil at low reynolds number—a review. *AIP Advances*, 11(5):050701, 2021.